

Unimolecular Photoconversion of Multicolor Luminescence on Hierarchical Self-Assemblies

Liangliang Zhu,[†] Xin Li,[‡] Quan Zhang,[†] Xing Ma,[§] Menghuan Li,[§] Huacheng Zhang,[†] Zhong Luo,[†] Hans Ågren,[‡] and Yanli Zhao^{*,†,§}

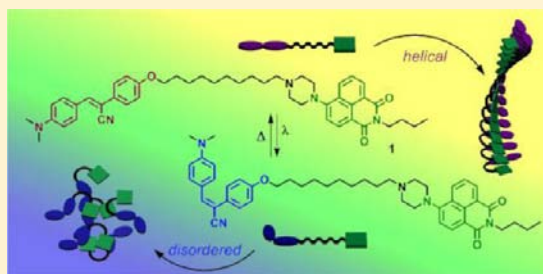
[†]Division of Chemistry and Biological Chemistry, School of Physical and Mathematical Sciences, Nanyang Technological University, 21 Nanyang Link, 637371, Singapore

[‡]Department of Theoretical Chemistry and Biology, School of Biotechnology, KTH Royal Institute of Technology, SE-10691 Stockholm, Sweden

[§]School of Materials Science and Engineering, Nanyang Technological University, 50 Nanyang Avenue, 639798, Singapore

S Supporting Information

ABSTRACT: Facile tuning of photophysical properties is highly desirable for boosting the performance and versatility of photoluminescent materials. In an attempt to overcome the challenge of achieving the photoswitching of multicolor luminescence on unimolecular platforms, we here report a novel hierarchical self-assembly of a cyanostilbene–naphthalimide dyad as the realization of phototunable luminescence at the unimolecular level. The work takes advantage of the photoisomerization of the cyanostilbene moiety from the *Z* form to its *E* form, which causes a morphological disorder in the molecular self-assembly and gives rise to a dual fluorescent characteristic accompanied by a progressive luminescent color conversion from yellow to green and finally to blue. Such systems with convertible multicolor luminescence might exhibit application potentials for unimolecular selective imaging and labeling, as exemplified by the cell imaging studies presented in this work.



INTRODUCTION

π -Conjugated organic luminophores with diverse emission colors and reversible responsivity to external stimuli are prospective materials for applications in numerous areas like biological imaging,¹ light emitting diodes,² photovoltaic cells,³ and sensors.⁴ In particular, rational designs capable of luminescent color conversion through externally stimulated controlling exhibit promising potentials for fabrication of intelligent materials with variable emissive properties.⁵ While effective switching of luminescent color has largely relied on hybrid materials or heterogeneous systems,⁵ the realization of in situ tuning of multicolor emission on a unimolecular scaffold remains a great challenge, because the design of a versatile conjugated backbone or the integration of several tunable luminophores with different color expressions into a single molecule is extremely difficult to achieve.⁶

On this basis, we propose in the present work a new strategy of taking advantage of regulated photophysical behavior of ordered molecular self-assemblies to overcome the above-mentioned limitations. Generally, a hierarchical supramolecular architecture formed in a certain environment shows properties distinct from those of their individual constituent molecules, and research on ordered molecular assemblies has therefore formed a very important topic in numerous scientific fields.⁷ Thanks to the morphological change that is reversibly switched by external stimuli and accompanied by the variation of a

certain property or signal, several examples of dynamically functional materials have recently been demonstrated.^{7,8} Inspired by these encouraging findings, we envision that the control of luminescent wavelength and color can be achieved at the unimolecular level by utilizing ordered molecular self-assemblies as observed in several photophysical studies.⁹

To realize this supposition, there are two key factors that need to be taken into account: (1) an integral molecular design for a solvent-triggered ordered self-assembly; and (2) a controllable in situ tuning ability for the morphology change together with the luminescent color conversion. Cyanostilbene and its derivatives are a group of light-responsive molecules on which the *Z/E*-isomerization can usually be applied for adjusting their emission wavelength and intensity.^{5a,10} Naphthalimide derivatives are typical donor– π –acceptor dyes, the emission wavelength of which is sensitive to the solvent environment.¹¹ We imagine that the planarity and the strength of π – π stacking from cyanostilbene and naphthalimide might be favorable for the formation of ordered architectures. With this in mind, we synthesized a novel dual-luminophore dyad (compound 1) by bridging *Z*-4-dimethylamino-cyanostilbene and 4-piperazinyl-1,8-naphthalimide with 1,10-decylene as shown in Figure 1a. The long alkyl chain was introduced to

Received: January 15, 2013

Published: March 14, 2013

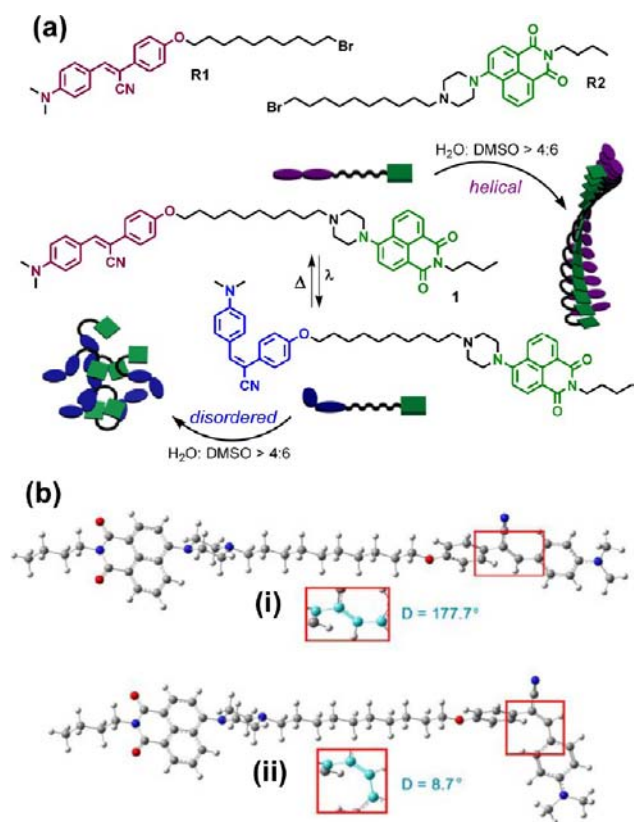


Figure 1. (a) Chemical structures of compounds **R1**, **R2**, and **1**, *Z/E* isomerization of the cyanostilbene unit in compound **1**, and a schematic representation of the corresponding helical and disordered assemblies of the *Z*-isomer and *E*-isomer, assisted by the solvent polarity. (b) Optimized conformational (i) *Z*- and (ii) *E*-forms of **1** at the B3LYP/6-31G* level of theory.

minimize electron transfer between the two luminophores so that their independent excitations can be exhibited in both the *Z*- and the *E*-isomers, as confirmed by the precalculations (Tables S1–S3 and Figure S1 in the Supporting Information). Reference compounds **R1** and **R2** with an isolated monofluorophore were also prepared for control experiments (we refer to the Experimental Section and Figure S2 in the Supporting Information for the synthetic routes of these compounds).

Helical assemblies are hierarchical architectures that have typically arisen from intermolecular self-assembly of small chiral building blocks.^{8a,b,12} However, achiral monomers can also form helical aggregates in some cases,¹³ for example, molecules containing a piperazinyl unit.¹⁴ In our current study, the piperazinyl group was introduced into compound **1** to permit a tendency toward spatial asymmetry. Such design is favorable for the production of a helical hierarchical conformation with strongly regulated emission color that can be followed by the tuning of *Z/E*-isomerization of the cyanostilbene unit along with the morphology change.

RESULTS AND DISCUSSION

Photocontrolled *Z/E*-Isomerization. In the initial state, the cyanostilbene unit in compound **1** adopts a *Z*-form evidenced by well-assigned ¹H NMR signals (Figure S3a in the Supporting Information). The *Z*-to-*E* photoisomerization occurs when the compound is irradiated by UV light at 254 nm.^{5a,15} The resultant *E*-isomer was confirmed by the ¹H NMR

spectrum where a group of upfield shifted resonances of the cyanostilbene unit along with no shifts of other protons were observed (Figure S3b in the Supporting Information). The ESI–MS spectrum of **1** did not show any new peaks after photoirradiation in comparison with that of the *Z*-isomer (Figure S4 in the Supporting Information), indicating that photoirradiation indeed promotes the *Z*-to-*E* isomerization of the cyanostilbene moiety rather than any other kind of photochemical reaction. According to the NMR integral studies, the ratio between the two isomers is 75:25 at the photostationary state under the illumination conditions. Similar to other photoisomerizable species,¹⁶ the *Z*-to-*E* photoisomerization of compound **1** remarkably diminishes the maximum absorption band of the molecule. This phenomenon can also be observed in high-polarity mixed solutions (see the corresponding absorption studies in the Supporting Information). Most of the *E*-isomer molecules can be converted back to the *Z*-form by heating the sample at high temperature over 100 °C (Figure S3c in the Supporting Information).

Luminescent spectral studies reveal that compound **1** is able to exhibit a dual-fluorescence feature, showing the appearance of a hypsochromically shifted and significantly intensified emission in the blue spectral region induced by the *Z*-to-*E* photoisomerization of the cyanostilbene unit. The shift of the emissive wavelength is confirmed by the calculated excitation energy difference of the cyanostilbene moiety (Figure S1 in the Supporting Information). Such a phenomenon can also be clearly featured by the control study of using **R1**. As seen from Figure S5 in the Supporting Information, the *E*-isomer of cyanostilbene in **R1** produces a strong emission at ~435 nm as compared to relatively quenched emission in its *Z*-isomer.

The change in fluorescent intensity is related to conformational restrictions of the cyanostilbene moiety. It has been established by previous experimental and theoretical studies¹⁷ that the twisting motion of the dimethylaminophenyl group is responsible for the formation of the twisted intramolecular charge transfer (TICT) state in dimethylaminobenzophenone and julolidine malononitrile. Our computational studies at the B3LYP/6-31G* level of theory indicate that the dihedral angle around the C=C double bond in cyanostilbene is 177.7° in its *Z*-isomer, and that the corresponding end-to-end distance of C=C=C-C is 3.91 Å. This conformation allows intramolecular rotation of the phenylamine group without steric hindrance from the opposite phenoxy group, resulting in efficient nonradiative decay pathway via the TICT state within cyanostilbene responsible for the fluorescence quenching.^{5a,15} Upon photoisomerization to the *E*-isomer, a relatively rigid conformation was formed with a C=C dihedral angle of 8.7° (Figure 1b) and a C=C=C-C end-to-end distance of 3.27 Å. The conformational energy of the *E*-isomer is higher than that of the *Z*-isomer, arising from steric hindrance between the phenylamine and phenoxy groups in cyanostilbene. Intramolecular rotation of the phenylamine group and the TICT pathway were thus suppressed, and a strong emission in the blue spectral region was observed for the *E*-isomer.^{5a,15}

Hierarchical Self-Assemblies. First, we explored the emission properties of compound **1** in different solvents because the solvent condition is a key factor for molecular self-assembly. As seen from Figure 2a, the emission of **1** was shifted bathochromically upon increasing the solvent polarity, along with a solvatochromic behavior of its absorption band (Figure S6 in the Supporting Information). Because neither the *Z*-form nor the *E*-form of this cyanostilbene unit shows aggregate

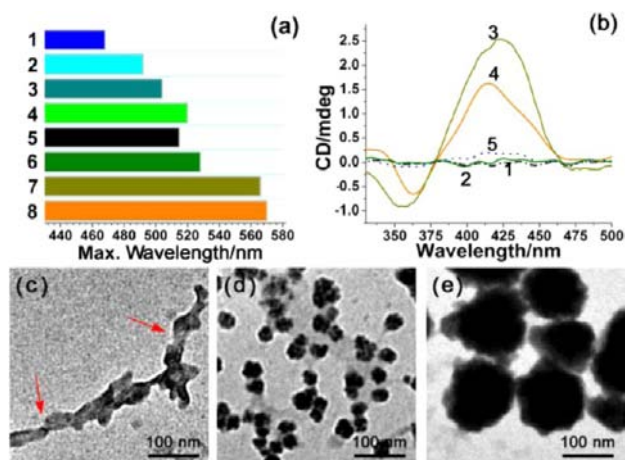


Figure 2. (a) The maximum emission wavelength of compound **1** under different solvent conditions: in (1) *n*-hexane, (2) toluene, (3) THF, (4) ethylene glycol, (5) DMSO, (6) DMSO with 20% water, (7) DMSO with 60% water, and (8) DMSO with 90% water. (b) Circular dichroism spectra of compound **1** in (1) DMSO, (2) DMSO with 20% water, (3) DMSO with 60% water, (4) DMSO with 90% water, and (5) DMSO with 90% water after sufficient photoirradiation. All of these data were collected at the concentration of 0.01 mM at 298 K. (c–e) TEM images of compound **1** prepared from (c) DMSO with 90% water, (d) DMSO with 20% water, and (e) DMSO with 90% water after sufficient photoirradiation. The TEM samples were stained with 1% aqueous sodium phosphotungstate solution and then allowed to air-dry. Some clear helical twists were highlighted by arrows in (c).

induced emission enhancement (AIEE),¹⁰ that is, no emission is increased significantly upon increasing the content of water as seen from Figure S5 in the Supporting Information, the emission band of **1** in the initial state is mainly originated from

the excitation of the naphthalimide group. The one from the cyanostilbene unit is very weak under its initial *Z*-form; that is, its emission was quenched by the TICT process (see also the control study in Figure S7 in the Supporting Information).

Interestingly, the emission of **1** turns to yellow in DMSO/H₂O solution when the content of water exceeds 40% (see bars 7 and 8 at ~570 nm in Figure 2a and Figure S8 of the Supporting Information). This observation is different from other amino-conjugated naphthalimide compounds,¹¹ and the emission of the reference compound **R2** or even a mixture of **R1/R2** always remains in green spectral region regardless of the water content in the DMSO/H₂O mixture solution (Figure S9 in the Supporting Information). Correspondingly, the absorption of **1** features a similar dependence on solvents. The absorption was greatly red-shifted in high-polarity DMSO/H₂O mixture solution (see curve 7 in Figure S6 of the Supporting Information). These observations indicate that the photophysical properties of compound **1** are particularly solvent-dependent.

Next, we carried out the circular dichroism (CD) measurements of compound **1**. A strong positive Cotton effect at ~425 nm and a negative one at ~360 nm were observed in DMSO/H₂O solution with high water contents (curves 3 and 4 in Figure 2b), corresponding to the electronic transitions of the luminophores at the same absorption wavelength. However, there was no CD signal observed under other solvent conditions with relatively low polarity (curves 1 and 2 in Figure 2b). Because compound **1** itself is an achiral molecule, the observed CD signals suggest the formation of the helical self-assembly architectures under the specific solvent conditions. This macrochirality was further confirmed by TEM studies. Helical nanowires with an average cross-sectional diameter of 30 nm were observed from the TEM images of **1**

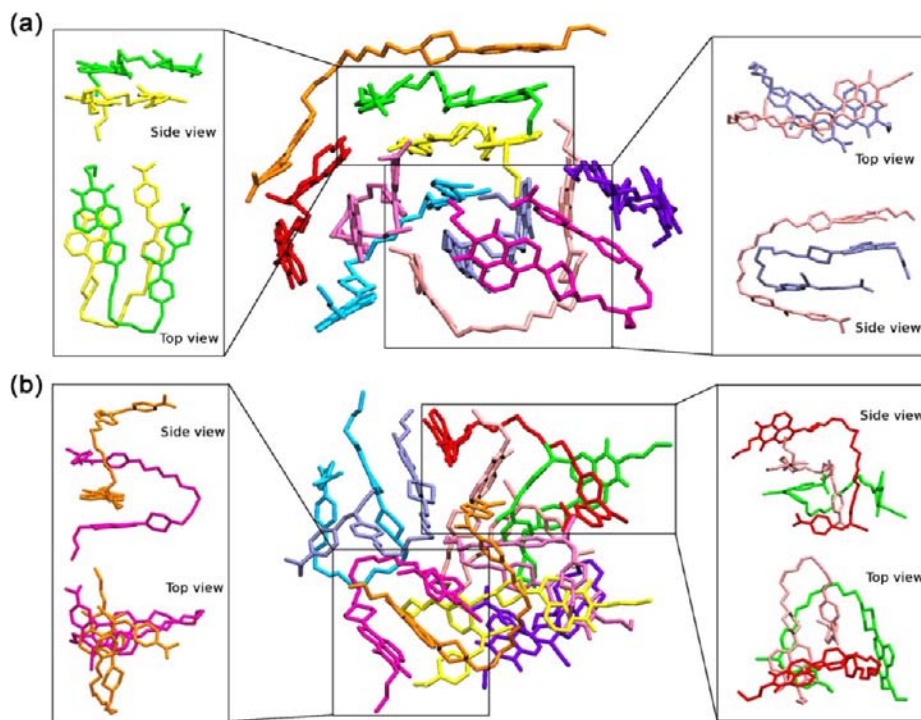


Figure 3. Snapshots of (a) hierarchical self-assembly conformation of **1** in *Z*-form under the environment of DMSO with 90% water and (b) disordered self-assembly conformation of **1** in *E*-form under the environment of DMSO with 90% water, from molecular dynamics (MD) simulations.

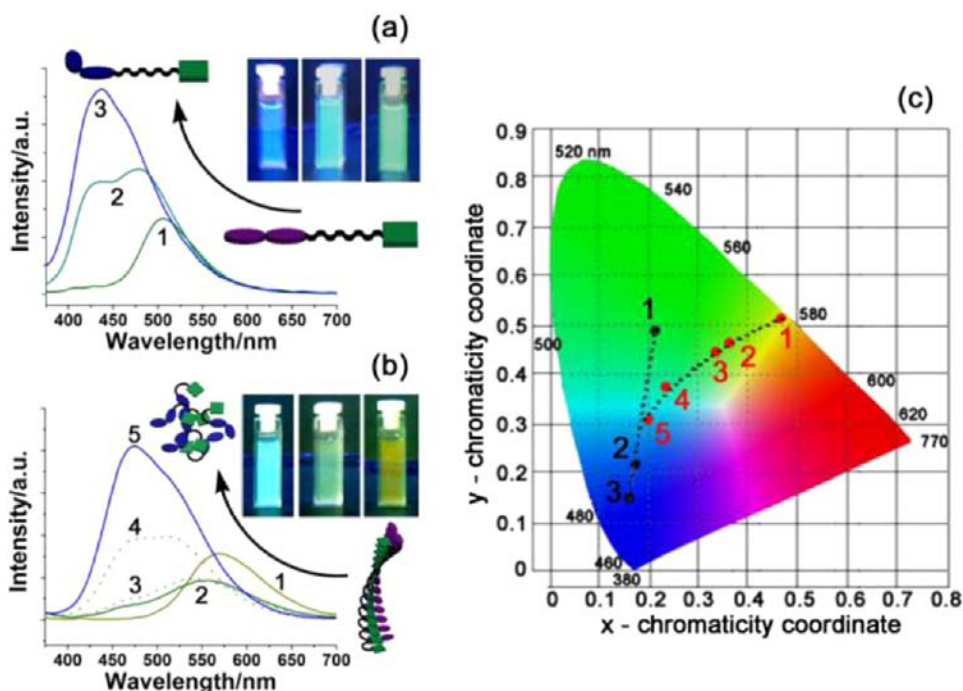


Figure 4. (a) Emission spectra ($\lambda_{\text{ex}} = 365$ nm) of compound **1** in THF at (1) initial state and after photoirradiation at 254 nm for (2) 3 h and (3) 6 h, and photo images (right-to-left) of the corresponding states 1, 2, and 3 under a UV light ($\lambda = 365$ nm). (b) Emission spectra ($\lambda_{\text{ex}} = 365$ nm) of compound **1** in DMSO with 90% water at (1) initial state and after photoirradiation at 254 nm for (2) 2 h, (3) 3 h, (4) 5 h, and (5) 8 h, and photo images (right-to-left) of the corresponding states 1, 2, and 5 under a UV light ($\lambda = 365$ nm). (c) CIE 1931 chromaticity diagram. The black dots signify the luminescent color coordinates for the corresponding states in (a), 1 (0.21, 0.49), 2 (0.17, 0.21), and 3 (0.16, 0.15), while the red dots feature the luminescent color coordinates for the corresponding states in (b), 1 (0.47, 0.51), 2 (0.36, 0.46), 3 (0.33, 0.45), 4 (0.23, 0.38), and 5 (0.20, 0.31).

prepared from a DMSO/H₂O (v:v = 10:90) mixture solution (Figure 2c and Figure S10a in the Supporting Information), while the spherical aggregates with an average spherical diameter of 40 nm were obtained from the sample when prepared in a DMSO/H₂O (v:v = 80:20) mixture solution (Figure 2d and Figure S10b in the Supporting Information). The nanowires reveal a clockwise helical stacking mode (*P*-helix), which is in agreement with the Cotton effect in the CD spectrum.¹⁸ On the other hand, none of **R1**, **R2**, and the mixture of **R1/R2** shows CD signals even in high-polarity mixture solution, demonstrating that the chirality can only be generated from compound **1**.

The red-shift of the emission in the hierarchical self-assembly of compound **1** could be assigned to an effect of *J*-aggregation,¹⁹ which causes the excited electron transferring from one molecule to the adjacent one (see the molecular simulations studies below). This process leads to an increase in the dipole moment of the self-assembly, which in turn allows the intermolecular charge transfer to extend over a large number of molecules, leading to significant bathochromic shift of the emission up to the yellow spectral region.^{19a}

Superstructures of Self-Assemblies. To gain further insight into the fine superstructures of the assemblies, molecular dynamics (MD) simulations were carried out to study the self-assembly behavior of compound **1**. It was found that in the presence of DMSO with 90% water, all molecules of **1** start to form aggregates, which were not observed in the simulations in pure DMSO solvent, in accordance with experimental observations. In the highly polar medium, the two π -conjugated fluorophores of each molecule seek suitable conformations that maximize the energetically favored π - π

stacking interactions;^{18b} that is, typically one molecule tends to adopt a U-shaped conformation to facilitate sufficient intra- or intermolecular stacking between the naphthalimide and cyanostilbene units (Figure 3a). It can be seen from Figure 3a that the layer-by-layer self-assembly of **1** in *Z*-form exhibits a distinguished hierarchical structure, indicative of the potential of forming advanced self-assembly architectures through further π - π stacking interactions (Figure 2c). It is inferred that the piperazine unit serves as a steric hindrance group, which enforces the naphthalimide unit to adopt a hierarchical spiral conformation. The resemblance between calculated CD spectra (Figure S11 in the Supporting Information) and experimental observations (Figure 2b) confirms the rationality and reliability of microscopic details provided by the theoretical simulations. The two reference compounds, **R1** and **R2**, were also studied by MD simulations under the same conditions. Neither **R1** nor **R2** was able to form stable aggregates. They only occasionally formed oligomeric assemblies (Figure S12 in the Supporting Information), which disintegrated after a short period of time. Thus, both naphthalimide and cyanostilbene units in compound **1** are required to provide a sufficient driving force for the collaborative formation of hierarchical architectures.

Upon irradiation at 254 nm, the ordered assembly became disordered on account of the *Z*-to-*E* photoisomerization of the cyanostilbene unit as indicated by the decrease of the CD signals (curve 5 in Figure 2b and Figure S11 in the Supporting Information) and by the morphology change from helical nanowires to spherical subjects (Figure 2e and Figure S10c in the Supporting Information). The *E*-form of **1** was also simulated using the same procedure as applied to its *Z*-form. However, the assembly did not show clear hierarchical structure

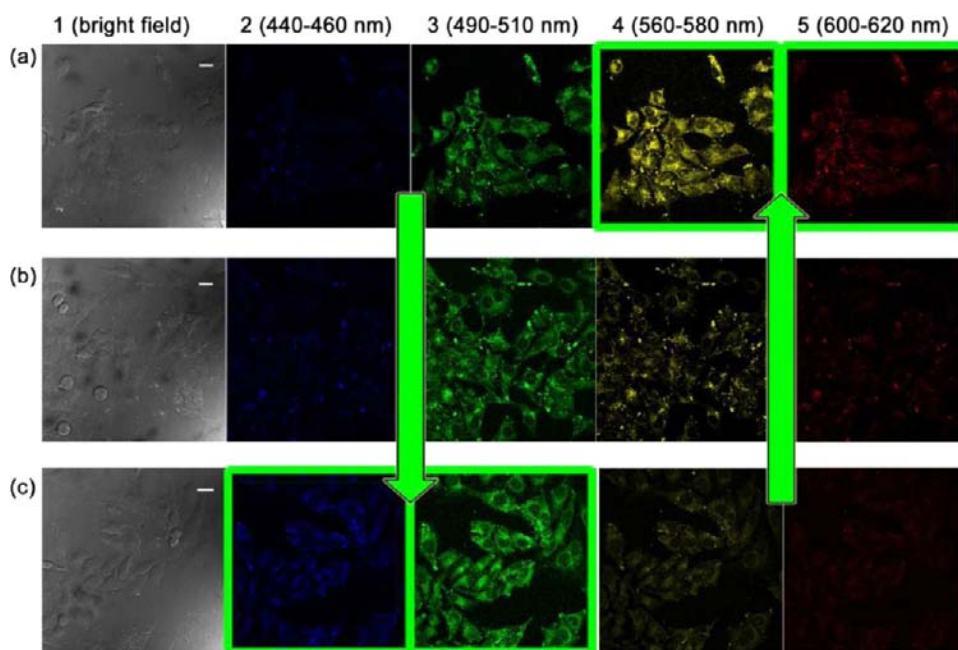


Figure 5. Representative results of the confocal fluorescence images for HeLa cells incubated with compound **1** in (a) initial state, (b) state after photoirradiation for 2 h, and (c) state after photoirradiation for 8 h, in DMEM medium containing 15% DMSO/PBS (pH 7.4, 1:49, v/v) at 37 °C. For each panel, the images from left to right were collected under different channels (readout wavelengths). The intensity changes of the same channels among the states were highlighted by arrows and frames. Scale bar, 20 μm .

due to the nonplanarity of the *E*-cyanostilbene unit (Figure 3b). In fact, the stacking direction of **1** in its *E*-form is not uniform as the whole assembly consists of several stacked subunits. Such a disordered assembly does not show obvious preference of further π - π stacking along a specific direction, in consistency with the spherical morphology of **1** in the *E*-form (Figure 2e). Although the computed solvent accessible surface area (Figure S13 in the Supporting Information) suggests that the aggregation degree of the self-assemblies is comparable between the *Z*- and *E*-forms, the order parameter²⁰ of the cyanostilbene and naphthalimide subunits averaged over the last 10 ns of the MD simulations is 0.46 in the *Z*-form and 0.09 in the *E*-form (Figure S14 in the Supporting Information). These results clearly show that the hierarchical superstructures of **1** in the *Z*-form are ordered self-assemblies and can be turned disordered by changing the compound into its *E*-form.

Multicolor Luminescent Conversion. The emission color of compound **1** in the initial state is green in some common solvents (e.g., THF), which mainly originated from the naphthalimide group discussed above (curve 1 in Figure 4a). Upon continuous irradiation by 254 nm UV light, the blue emission from the *E*-cyanostilbene unit gradually overwhelms the green fluorescence of the naphthalimide unit (curves 2 and 3 in Figure 4a). The track with black dots in the Commission Internationale de l'Éclairage (CIE) diagram shows that the range of the color conversion is between green and blue (Figure 4c). Interestingly, when the compound is in a high-polarity mixture solution, a totally different phenomenon is presented.

The above-mentioned hierarchical self-assembly of *Z*-formed **1** in DMSO with 90% water results in a significant bathochromic shift of the emission band, from green to yellow (curve 1 in Figure 4b). Upon irradiation at 254 nm over a period of time, the emission changes back to the green spectral region because of the variation of the self-assembly process

(curve 2 in Figure 4b). Continuous irradiation leads to an increase in the ratio of the *E*- to *Z*-isomers, resulting in further enhancement of the emission intensity of the *E*-cyanostilbene unit and corresponding changes of luminescent color from green to blue (curves 3, 4, and 5 in Figure 4b). Thus, multicolor luminescent conversion along yellow, green, and blue on this unimolecular dyad is realized by in situ photoirradiation, credited by the broadening of the color tuning range (see the track with red dots in the CIE diagram, Figure 4c) on account of the controllable hierarchical self-assembly. As the *E*-to-*Z* isomerization of the cyanostilbene unit is powered by heating, the corresponding emission can be recovered to some extent (Figure S15 in the Supporting Information). The quantum yields (QYs) for the initial state and the photostationary state of **1** are 5.5% and 28%, respectively, relative to the standard reference (Rhodamine B, $\Phi = 65\%$).²¹ In this way, the single entity might exhibit potentials for tunable light-emitting applications, as exemplified by the unimolecular selective imaging studies discussed below.

Unimolecular Selective Imaging Studies. Although tunable cell imaging has been emerging,²² reports on unimolecular selective imaging among detection channels are still scarce. In our work, experiments in living cells were also carried out to further demonstrate the potential application of the tunable multicolor luminescence provided from the dyad. On account of the biologically incompatible isomerization conditions (254 nm of irradiation or 100 °C of heating), we need to prepare the unimolecular samples with different states. Incubations of HeLa cells with compound **1** at the initial state and the compound after photoirradiation for 2 and 8 h, respectively, in a DMEM medium containing 15% DMSO/PBS (pH 7.4, 1:49, v/v) at 37 °C for 24 h, were monitored by the confocal microscopy (Figure 5). The results indicate that the different states of compound **1** can be all endocytosed by cells for bioimaging (see the images of bright field and each

luminescent channels for comparison) with relatively low cytotoxicity (Figure S16 in the Supporting Information).

Because of the complicated intracellular environments, it is very difficult to characterize the superstructures of the dyad inside the cells. Fortunately, the optical spectral information can provide key evidence for the self-assemblies. In our studies, we established fluorescence spectra of compound **1** on an intracellular platform by collecting and merging the emission intensities from different channels (see Figures S17–S24 in the Supporting Information). As seen from Figure S18b in the Supporting Information, the maximum intensity of **1** in the initial state in HeLa cells appears at the wavelength of ~ 570 nm, different from that of **R2** in HeLa cells (~ 500 nm, Figure S24b in the Supporting Information). As we demonstrated above, the hierarchical self-assemblies allow the emission of **1** to shift bathochromically to the yellow spectral region. In that case, we can deduce that such ordered superstructures of **1** in the initial state can still be kept inside the cells. Moreover, the microspectroscopies performed by using **1** in different states in HeLa cells are in agreement with their corresponding cuvette studies (Figure S25 in the Supporting Information). These results suggest that the self-assemblies in different states can also be well distinguished in the intracellular environments. This observation is reasonable because apparent isomerization of the compound would not take place at 37°C for 24 h (see the corresponding cuvette studies in Figure S26 of the Supporting Information).

The effect of unimolecular selective imaging can be detected by confocal microscopes. The cell imaging with compound **1** in the initial state can be clearly observed from the channels with the wavelength ranges of 560–580 nm and 600–620 nm, while the imaging of the same channels turns to dark with **1** in the photostationary states (Figure 5). In contrast, the imaging with compound **1** in the initial state is relatively weak from the channels with wavelengths of 440–460 and 490–510 nm, whereas it is strengthened with **1** in the photostationary states (Figure 5). The variation of the cell imaging can also be observed from a conventional fluorescence microscopy. The cell imaging with **1** in the photostationary state can still be acquired from the DAPI (4',6-diamidino-2-phenylindole) channel, whereas the one with **1** in the initial state is dark (see Figure S27 in the Supporting Information). All of these alternations among the channels can be explained by the unimolecular emission wavelength shifts. Such spectrally tunable unimolecular entities might present a promising potential for the applications of advanced bioimaging and labeling.

CONCLUSION

A novel cyanostilbene–naphthalimide dyad with tunable photophysical behavior has been developed. Solvent-dependent helical hierarchical architectures have been constructed through self-assembly of the compound in DMSO with high water content. The well-ordered molecular arrangement leads to a significant bathochromic shift of the initial emission band from the green to the yellow spectral region. On this basis, a conversion of luminescent color along yellow, green, and blue has been achieved by utilizing the self-assembly disorder and the dual fluorescent characteristic originated from the *Z*-to-*E* photoisomerization of the cyanostilbene unit. We emphasize that the photoconversion of multicolor luminescence has been carried out on the unimolecular entity. Unimolecular selective imaging studies using this unique compound have been

successfully carried out at the intracellular level. The ramifications of the present results are valuable for the design of smart systems with luminescent color tuning properties and potential applications in tunable light-emitting cases.

EXPERIMENTAL SECTION

General. ^1H NMR and ^{13}C NMR spectra were measured on a Bruker BBFO-400 spectrometer. The electronic spray ionization (ESI) mass spectra were recorded on a ThermoFinnigan LCQ quadrupole ion trap mass spectrometer. High-resolution mass spectrometry (HR-MS) was performed on a Waters Q-tof Premier MS spectrometer. Absorption spectra were recorded on a Shimadzu UV-3600 UV–vis–NIR spectrophotometer, while the fluorescent emission spectra were recorded on a Varian Cary Eclipse fluorescence spectrophotometer. The CD spectra were recorded on a Jasco J-810 CD spectrophotometer using a 1 cm quartz cell. The photoirradiation was carried on an ENF-260C/FBE UV lamp (15 W) with the irradiation wavelength of 254 nm in a 1 cm quartz cell. TEM images were collected on a JEM-1400 (JEOL) operated at 100–120 kV. Melting points were determined by using an OptiMelt automated melting point system. The photo images were photographed by a Nikon COOLPIX S8000 digital camera. The confocal microscopic images were captured by LEICA TCS SPS confocal microscope, while the fluorescence microscopic images were taken using a Nikon D-Eclipse C1 microscope.

Synthesis of Compound 3. The preparation for this compound was according to a similar procedure described in literature.²³

Synthesis of Compounds 2 and R1. These compounds were prepared according to our previous report.^{5a}

Synthesis of Compound R2. Compound **3** (1.24 g, 3.68 mmol) was added to a DMF solution (6 mL) containing 1,10-dibromoethane (10.0 g, 33.3 mmol). The mixture solution was then added with K_2CO_3 (1.0 g, 7.25 mmol). The solution was stirred for 8 h at 80°C under Ar protection. It then was poured into deionized water (30 mL) and kept overnight. After filtration, the crude solid was collected and then purified through silica gel chromatography (petroleum ether:ethyl acetate = 3:1) to afford yellow compound **R2** (1.38 g, 67.4%). mp 79 – 80°C . ^1H NMR (400 MHz, CDCl_3 , 298 K): δ = 8.60 (dd, J_1 = 7.2 Hz, J_2 = 1.2 Hz, 1H), 8.53 (d, J = 8.0 Hz, 1H), 8.42 (dd, J_1 = 8.4 Hz, J_2 = 1.2 Hz, 1H), 7.70 (dd, J_1 = 8.4 Hz, J_2 = 7.2 Hz, 1H), 7.23 (d, J = 8.0 Hz, 1H), 4.19 (t, J = 7.6 Hz, 2H), 3.43 (t, J = 7.2 Hz, 2H), 3.32 (br, 4H), 2.79 (br, 4H), 2.50 (t, J = 8.0 Hz, 2H), 1.88 (m, 2H), 1.74 (m, 2H), 1.58 (m, 2H), 1.47 (m, 2H), 1.33 (m, 12H), 0.99 (t, J = 7.6 Hz, 3H). ^{13}C NMR (100 MHz, CDCl_3 , 298 K): δ = 164.53, 163.06, 156.00, 132.55, 131.03, 130.26, 129.90, 126.18, 125.57, 123.34, 116.74, 114.88, 58.79, 53.34, 53.10, 40.09, 34.03, 32.83, 30.28, 29.54, 29.47, 29.39, 28.75, 28.17, 27.56, 26.92, 20.41, 13.87. HRMS (ESI) m/z : $[\text{M} + \text{H}]^+$ calcd for $\text{C}_{30}\text{H}_{43}\text{N}_3\text{O}_2\text{Br}_2$, 556.2539; found m/z , 556.2528.

Synthesis of Compound 1. A mixture solution of compound **2** (0.43 g, 1.63 mmol), **R2** (0.9 g, 1.62 mol), and K_2CO_3 (450 mg, 3.26 mmol) in acetone (15 mL) was refluxed for 11 h and then poured into EtOH (100 mL). The crude solid was immediately precipitated and sufficiently washed by *n*-hexane, deionized water, and EtOH, respectively, providing yellow compound **1** (0.89 mg, 74.3%). mp 118 – 120°C . ^1H NMR (400 MHz, CDCl_3 , 298 K): δ = 8.60 (dd, J_1 = 7.2 Hz, J_2 = 0.8 Hz, 1H), 8.53 (d, J = 8.0 Hz, 1H), 8.42 (dd, J_1 = 8.4 Hz, J_2 = 0.8 Hz, 1H), 7.83 (d, J = 9.2 Hz, 2H), 7.70 (dd, J_1 = 8.4 Hz, J_2 = 7.2 Hz, 1H), 7.56 (d, J = 8.4 Hz, 2H), 7.31 (s, 1H), 7.22 (d, J = 8.0 Hz, 1H), 6.94 (d, J = 8.8 Hz, 2H), 6.73 (d, J = 8.8 Hz, 2H), 4.19 (t, J = 7.6 Hz, 2H), 4.01 (t, J = 6.4 Hz, 2H), 3.32 (br, 4H), 3.07 (s, 6H), 2.79 (br, 4H), 2.50 (t, J = 8.0 Hz, 2H), 1.82 (m, 2H), 1.74 (m, 2H), 1.57 (m, 2H), 1.47 (m, 2H), 1.36 (m, 12H), 0.99 (t, J = 7.6 Hz, 3H). ^{13}C NMR (100 MHz, CDCl_3 , 298 K): δ = 164.54, 164.22, 164.06, 163.40, 159.17, 158.47, 156.02, 153.86, 151.42, 148.13, 140.64, 138.42, 132.56, 132.18, 131.02, 130.91, 130.28, 129.90, 127.94, 126.71, 126.18, 125.56, 123.33, 122.04, 121.91, 119.56, 116.72, 116.48, 114.86, 111.66, 104.53, 68.16, 58.81, 53.35, 53.11, 40.07, 30.29, 29.56, 29.50, 29.34, 29.21, 27.58, 26.94, 26.02, 20.42, 13.87. HRMS (ESI) m/z : $[\text{M} + \text{H}]^+$ calcd for $\text{C}_{47}\text{H}_{58}\text{N}_5\text{O}_3$, 740.4540; found m/z , 740.4495.

MTT Cytotoxicity Assay. The cytotoxicity was evaluated by an MTT assay. HeLa cells were seeded into a 96-well plate at a density of 1×10^4 cells/well in DMEM medium. After the cells were grown for 24 h, the medium was changed into a new medium (100 μ L/well) containing various concentrations (diluted from a solution of DMSO/PBS (pH 7.4, 1:49, v/v)) of compound **1** at the initial state and of the compound after sufficient photoirradiation. The cells then were incubated for another 24 h before conducting MTT assay by replacing the medium with new medium containing MTT (100 μ L, 0.5 mg mL⁻¹). After incubation for 4 h, the medium was removed, and DMSO (100 μ L) was added into each well. The plate was gently shaken for 15 min, and the corresponding absorbance intensity at 565 nm was recorded using a microplate reader (infinite 200 PRO, Tecan). The relative cell viability related to control wells that were only treated with medium was calculated by $[A]_{\text{test}}/[A]_{\text{control}}$ where $[A]_{\text{test}}$ and $[A]_{\text{control}}$ are the average absorbances of the test and control samples, respectively.

Confocal Microscopic Images. HeLa cells were seeded in 35 mm plastic-bot-tomed m-dishes and grown in a DMEM medium for 24 h. The cells then were treated with compound **1** (10^{-6} M) at the initial state and the compound after photoirradiation for 2 and 8 h, respectively. After another 24 h incubation, the medium was removed, and the cells were washed with a PBS buffer (pH 7.4) three times and fixed with 4.0% formaldehyde at room temperature for 15 min. After 4.0% formaldehyde was removed and washing with PBS buffer (pH 7.4) three times, the fluorescence images of the cells were captured using a confocal microscope with different channels. The intensity of all of these channels was read under the same gain.

Fluorescence Microscopic Images. HeLa cells were seeded in 35 mm plastic-bot-tomed m-dishes and grown in a DMEM medium for 24 h. The cells then were treated with compound **1** (10^{-6} M) at the initial state and the compound (10^{-6} M) after sufficient photoirradiation, respectively. After another 24 h incubation, the medium was removed, and the cells were washed with PBS buffer (pH 7.4) three times and fixed with 4.0% formaldehyde at room temperature for 15 min. After 4.0% formaldehyde was removed and washing with PBS buffer (pH 7.4) three times, the fluorescence images of the cells were captured using a fluorescence microscope with DAPI and FITC channels.

Computational Details. The theoretical computations consist of three steps: (1) quantum chemical calculations of a single molecule of compound **1**, (2) molecular dynamics simulations of 10 molecules forming a self-assembly, and (3) semiempirical calculations of electronic circular dichroism spectra of the self-assembly. First, conformational geometries of the *Z*- and *E*-forms of compound **1** were optimized by density functional theory calculations with the hybrid B3LYP functional²⁴ and the 6-31G* basis set²⁵ as implemented in the Gaussian 09 program.²⁶ Subsequent time-dependent density functional theory (TDDFT) calculations with the CAM-B3LYP functional²⁷ and the 6-31G* basis set were then carried out at the optimized geometries of *Z*- and *E*-forms of **1**, to gain information of excitation energies of the fluorophores. In the TDDFT calculations, the solvent effects of DMSO were taken into account by the polarizable continuum model (PCM).²⁸ Computational results from the TDDFT calculations, summarized in Tables S1–S3 and Figure S1 of the Supporting Information, indicate that the naphthalimide and cyanostilbene moieties are excited independently within a single molecule of **1**. Second, molecular dynamics simulations were performed by the GROMACS program package²⁹ employing the general Amber force field (GAFF)³⁰ for both the *Z*- and *E*-forms of compound **1** with RESP³¹ partial atomic charges derived from the electrostatic potentials computed at the HF/6-31G* level of theory. Here, the equilibrium bond lengths, bond angles, as well as the force constants for the dihedral potentials were further refined so that the molecular mechanical force field could well reproduce the quantum chemically predicted geometries (Figure S28 in the Supporting Information). For each form of compound **1**, 10 molecules were first simulated in pure DMSO solvent under constant-*NpT* conditions ($T = 298$ K, $p = 1$ atm) for 10 ns, then 90% of DMSO was replaced by water with the same volume and the simulation was continued for 50

ns. Both the *Z*- and the *E*-forms of **1** were found to form self-assemblies in mixed DMSO/H₂O (1:9) solution, and their solvent accessible surface areas (Figure S13 in the Supporting Information) were computed using the *g_sas* tool of the GROMACS program package.²⁹ It was observed that the solvent accessible surface area of the *Z*-form self-assembly becomes stable during 40–50 ns, and that the solvent accessible surface area of the *E*-form self-assembly is stable within 30–50 ns. In the third step, 20 snapshots were extracted from the last 10 ns trajectory of the *Z*-form self-assembly with equal time interval, and 40 snapshots were extracted from the last 20 ns trajectory of the *E*-form self-assembly. In each snapshot, the long alkyl chains were removed and the remaining dangling bonds were saturated with hydrogen atoms, because these alkyl chains do not contribute to the CD spectra in the region of 300–500 nm. The rest of the self-assembly, consisting of the naphthalimide and cyanostilbene units, was fed into semiempirical Zindo/S calculations³² to compute the CD spectra, and these spectra were averaged for the *Z*- and *E*-form self-assemblies of **1**, respectively (Figure S11 in the Supporting Information). To assess the orderedness of the self-assembly, the order parameter of the self-assembly consisting of the naphthalimide and cyanostilbene units in each snapshot was computed according to a previously reported method.²⁰ The computed order parameters, shown in Figure S14 of the Supporting Information, reflect the different stacking mode and optical rotation properties of the *Z*- and *E*-form self-assemblies of compound **1**.

■ ASSOCIATED CONTENT

📄 Supporting Information

Conformational geometries of compound **1**, characterization spectra of **1**, supplementary optical studies, TEM images with a relatively large scale, supplementary calculation data for molecular dynamics simulations, MTT cytotoxic study, intracellular microspectroscopies measured by confocal microscopes, cell imaging observed from a fluorescence microscopy, and full citation for ref 26. This material is available free of charge via the Internet at <http://pubs.acs.org>.

■ AUTHOR INFORMATION

Corresponding Author

zhaoyanli@ntu.edu.sg

Notes

The authors declare no competing financial interest.

■ ACKNOWLEDGMENTS

This work was financially supported by the Singapore National Research Foundation Fellowship (NRF2009NRF-RF001-015), Singapore National Research Foundation CREATE program—Singapore Peking University Research Centre for a Sustainable Low-Carbon Future, and the Centre of Excellence for Silicon Technologies (A*Star SERC no.: 112 351 0003). L.Z. is grateful for helpful suggestions from Ms. K. T. Nguyen and Dr. H. Yan. X.L. acknowledges a grant from the Carl Tryggers Foundation and computational resources provided by the Swedish National Infrastructure for Computing for the project “Multiphysics Modeling of Molecular Materials”, SNIC 022/09-25.

■ REFERENCES

- (1) (a) Li, Z.; Barnes, J. C.; Bosoy, A.; Stoddart, J. F.; Zink, J. I. *Chem. Soc. Rev.* **2012**, *41*, 2590–2605. (b) You, Y.; Lee, S.; Kim, T.; Ohkubo, K.; Chae, W.-S.; Fukuzumi, S.; Jhon, G.-J.; Nam, W.; Lippard, S. J. *J. Am. Chem. Soc.* **2011**, *133*, 18328–18342. (c) Bouffard, J.; Kim, Y.; Swager, T. M.; Weissleder, R.; Hilderbrand, S. A. *Org. Lett.* **2008**, *10*, 37–40. (d) Bharali, D. J.; Klejbor, I.; Stachowiak, E. K.; Dutta, P.; Roy,

- I.; Kaur, N.; Bergey, E. J.; Prasad, P. N.; Stachowiak, M. K. *Proc. Natl. Acad. Sci. U.S.A.* **2005**, *102*, 11539–11544.
- (2) (a) D'Andrade, B. W.; Forrest, S. R. *Adv. Mater.* **2004**, *16*, 1585–1595. (b) Zuniga, C. A.; Barlow, S.; Marder, S. R. *Chem. Mater.* **2011**, *23*, 658–681. (c) Al-Attar, H. A.; Griffiths, G. C.; Moore, T. N.; Tavassli, M.; Fox, M. A.; Bryce, M. R.; Monkman, A. P. *Adv. Funct. Mater.* **2011**, *21*, 2376–2382. (d) Wang, L.; Wong, W.-Y.; Lin, M.-F.; Wong, W.-K.; Cheah, K.-W.; Tam, H.-L.; Chen, C. H. *J. Mater. Chem.* **2008**, *18*, 4529–4536. (e) Hsu, C.-W.; Lin, C.-C.; Chung, M.-W.; Chi, Y.; Lee, G.-H.; Chou, P.-T.; Chang, C.-H.; Chen, P.-Y. *J. Am. Chem. Soc.* **2011**, *133*, 12085–12099.
- (3) (a) Yella, A.; Lee, H.-W.; Tsao, H. N.; Yi, C.; Chandiran, A. K.; Nazeeruddin, M. K.; Diau, E. W.-G.; Yeh, C.-Y.; Zakeeruddin, S. M.; Grätzel, M. *Science* **2011**, *334*, 629–634. (b) Kim, J. Y.; Lee, K.; Coates, N. E.; Moses, D.; Nguyen, T.-Q.; Dante, M.; Heeger, A. J. *Science* **2007**, *317*, 222–225. (c) Schlenker, C. W.; Thompson, M. E. *Chem. Commun.* **2011**, *47*, 3702–3716. (d) Thompson, B. C.; Fréchet, J. M. J. *Angew. Chem., Int. Ed.* **2007**, *47*, 58–77.
- (4) (a) de Silva, A. P.; Uchiyama, S. *Nat. Nanotechnol.* **2007**, *2*, 399–410. (b) Kim, H. N.; Guo, Z. Q.; Zhu, W. H.; Yoon, J.; Tian, H. *Chem. Soc. Rev.* **2011**, *40*, 79–93. (c) Guliyev, R.; Coskun, A.; Akkaya, E. U. *J. Am. Chem. Soc.* **2009**, *131*, 9007–9013.
- (5) (a) Zhu, L.; Ang, C. Y.; Li, X.; Nguyen, K. T.; Tan, S. Y.; Ågren, H.; Zhao, Y. *Adv. Mater.* **2012**, *24*, 4020–4024. (b) Sagara, Y.; Kato, T. *Angew. Chem., Int. Ed.* **2008**, *47*, 5175–5178. (c) Zhang, X.; Rehm, S.; Safont-Sempere, M. M.; Würthner, F. *Nat. Chem.* **2009**, *1*, 623–629.
- (6) Zuccherro, A. J.; McGrier, P. L.; Bunz, U. H. F. *Acc. Chem. Res.* **2010**, *43*, 397–408.
- (7) (a) Whitesides, G. M.; Grzybowski, B. *Science* **2002**, *295*, 2418–2421. (b) Kinbara, K.; Aida, T. *Chem. Rev.* **2005**, *105*, 1377–1400. (c) Lehn, J. M. *Science* **2002**, *295*, 2400–2403. (d) Aida, T.; Meijer, E. W.; Stupp, S. I. *Science* **2012**, *335*, 813–817. (e) Kiyonaka, S.; Sada, K.; Yoshimura, I.; Shinkai, S.; Kato, N.; Hamachi, I. *Nat. Mater.* **2004**, *3*, 58–64.
- (8) (a) Korevaar, P. A.; George, S. J.; Markvoort, A. J.; Smulders, M. M. J.; Hilbers, P. A. J.; Schenning, A. P. H. J.; De Greef, T. F. A.; Meijer, E. W. *Nature* **2012**, *481*, 492–496. (b) Kim, H.-J.; Kang, S.-K.; Lee, Y.-K.; Seok, C.; Lee, J.-K.; Zin, W.-C.; Lee, M. *Angew. Chem., Int. Ed.* **2010**, *49*, 8471–8475. (c) Gröschel, A. H.; Schacher, F. H.; Schmalz, H.; Borisov, O. V.; Zhulina, E. B.; Walther, A.; Müller, A. H. E. *Nat. Commun.* **2012**, *3*, 710.
- (9) (a) Maggini, L.; Bonifazi, D. *Chem. Soc. Rev.* **2012**, *41*, 211–241. (b) Wong, K. M.-C.; Yam, V. W.-W. *Acc. Chem. Res.* **2011**, *44*, 424–434. (c) Hua, Y.; Flood, A. H. *J. Am. Chem. Soc.* **2010**, *132*, 12838–12840.
- (10) (a) An, B.-K.; Gierschner, J.; Park, S. Y. *Acc. Chem. Res.* **2012**, *45*, 544–554. (b) An, B.-K.; Gihm, S. H.; Chung, J. W.; Park, C. R.; Kwon, S.-K.; Park, S. Y. *J. Am. Chem. Soc.* **2009**, *131*, 3950–3957. (c) Zhu, L.; Zhao, Y. *J. Mater. Chem. C* **2013**, *1*, 1059–1065.
- (11) (a) Lin, H.-H.; Chan, Y.-C.; Chen, J.-W.; Chang, C.-C. *J. Mater. Chem.* **2011**, *21*, 3170–3177. (b) Meng, X.; Zhu, W.; Zhang, Q.; Feng, Y.; Tan, W.; Tian, H. *J. Phys. Chem. B* **2008**, *112*, 15636–15645. (c) Gan, J.-A.; Song, Q. L.; Hou, X. Y.; Chen, K.; Tian, H. *J. Photochem. Photobiol., A: Chem.* **2004**, *162*, 399–406.
- (12) Srinivasan, S.; Babu, P. A.; Mahesh, S.; Ajayaghosh, A. *J. Am. Chem. Soc.* **2009**, *131*, 15122–15123.
- (13) (a) Yuan, W. Z.; Mahtab, F.; Gong, Y.; Yu, Z.-Q.; Lu, P.; Tang, Y.; Lam, J. W. Y.; Zhu, C.; Tang, B. Z. *J. Mater. Chem.* **2012**, *22*, 10472–10479. (b) Qu, S.; Wang, L.; Liu, X.; Li, M. *Chem.-Eur. J.* **2011**, *17*, 3512–3518.
- (14) Yu, S.-Y.; Zhang, Z.-X.; Cheng, E. C.-C.; Li, Y.-Z.; Yam, V. W.-W.; Huang, H.-P.; Zhang, R. *J. Am. Chem. Soc.* **2005**, *127*, 17994–17995.
- (15) (a) Zhu, L.-L.; Li, X.; Ji, F.-Y.; Ma, X.; Wang, Q.-C.; Tian, H. *Langmuir* **2009**, *25*, 3482–3486. (b) Zhu, L.-L.; Qu, D.-H.; Zhang, D.; Chen, Z.-F.; Wang, Q.-C.; Tian, H. *Tetrahedron* **2010**, *66*, 1254–1260.
- (16) (a) Zhu, L.; Yan, H.; Nguyen, K. T.; Tian, H.; Zhao, Y. *Chem. Commun.* **2012**, *48*, 4290–4292. (b) Yan, H.; Teh, C.; Sreejith, S.; Zhu, L.; Kwok, A.; Fang, W.; Ma, X.; Nguyen, K. T.; Korzh, V.; Zhao, Y. *Angew. Chem., Int. Ed.* **2012**, *51*, 8373–8377. (c) Zhu, L.; Ma, X.; Ji, F.; Wang, Q.; Tian, H. *Chem.-Eur. J.* **2007**, *13*, 9216–9222.
- (17) (a) Grabowski, Z. R.; Rotkiewicz, K.; Rettig, W. *Chem. Rev.* **2003**, *103*, 3899–4031. (b) Singh, A. K.; Ramakrishna, G.; Ghosh, H. N.; Palit, D. K. *J. Phys. Chem. A* **2004**, *108*, 2583–2597. (c) Zhang, W.; Lan, Z.; Sun, Z.; Gaffney, K. J. *J. Phys. Chem. B* **2012**, *116*, 11527–11536.
- (18) (a) Lu, X.; Guo, Z.; Sun, C.; Tian, H.; Zhu, W. *J. Phys. Chem. B* **2011**, *115*, 10871–10876. (b) Danila, I.; Riobé, F.; Piron, F.; Puigmartí-Luis, J.; Wallis, J. D.; Linares, M.; Ågren, H.; Beljonne, D.; Amabilino, D. B.; Avarvari, N. *J. Am. Chem. Soc.* **2011**, *133*, 8344–8353.
- (19) (a) Adhikari, R. M.; Shah, B. K.; Palayangoda, S. S.; Neckers, D. C. *Langmuir* **2009**, *25*, 2402–2406. (b) Oelkrug, D.; Tompert, A.; Gierschner, J.; Egelhaaf, H.-J.; Hanack, M.; Hohloch, M.; Steinhuber, E. *J. Phys. Chem. B* **1998**, *102*, 1902–1907. (c) Yazdani, O.; Irandoust, M.; Ghasemi, J. B.; Hooshmand, S. *Dyes Pigm.* **2012**, *92*, 1031–1041.
- (20) Wilson, M. R. *J. Mol. Liq.* **1996**, *68*, 23–31.
- (21) Kubin, R. F.; Fletcher, A. N. *J. Lumin.* **1982**, *27*, 455–462.
- (22) (a) Wang, B.; Hai, J.; Liu, Z.; Wang, Q.; Yang, Z.; Sun, S. *Angew. Chem., Int. Ed.* **2010**, *49*, 4576–4579. (b) Shi, W.; Li, X.; Ma, H. *Angew. Chem., Int. Ed.* **2012**, *51*, 6432–6435. (c) Zhu, M.-Q.; Zhang, G.-F.; Li, C.; Aldred, M. P.; Chang, E.; Drezek, R. A.; Li, A. D. Q. *J. Am. Chem. Soc.* **2011**, *133*, 365–372.
- (23) Ren, J.; Zhao, X.-L.; Wang, Q.-C.; Ku, C.-F.; Qu, D.-H.; Chang, C.-P.; Tian, H. *Dyes Pigm.* **2005**, *64*, 179–186.
- (24) Becke, A. D. *J. Chem. Phys.* **1993**, *98*, 5648–5652.
- (25) Hehre, W. J.; Ditchfield, R.; Pople, J. A. *J. Chem. Phys.* **1972**, *56*, 2257–2261.
- (26) Frisch, M. J.; et al. *Gaussian 09*, revision A.2; Gaussian, Inc.: Wallingford, CT, 2009.
- (27) Yanai, T.; Tew, D.; Handy, N. *Chem. Phys. Lett.* **2004**, *393*, 51–57.
- (28) Tomasi, J.; Mennucci, B.; Cammi, R. *Chem. Rev.* **2005**, *105*, 2999–3093.
- (29) Hess, B.; Kutzner, C.; van der Spoel, D.; Lindahl, E. *J. Chem. Theory Comput.* **2008**, *4*, 435–447.
- (30) Wang, J.; Wolf, R. M.; Caldwell, J. W.; Kollman, P. A.; Case, D. A. *J. Comput. Chem.* **2004**, *25*, 1157–1174.
- (31) Bayly, C. I.; Cieplak, P.; Cornell, W.; Kollman, P. A. *J. Phys. Chem.* **1993**, *97*, 10269–10280.
- (32) Zerner, M. C. In *Reviews of Computational Chemistry*; Lipkowitz, K. B., Boyd, D. B., Eds.; VCH Publishing: New York, 1991; Vol. 2, pp 313–366.